Analysis of correlations and search for evidence of deterministic chaos in rhythmic motor control by the human brain

Sean Roberts and R. Eykholt
Department of Physics, Colorado State University, Fort Collins, Colorado 80523

Michael H. Thaut
Center for Biomedical Research in Music, Colorado State University, Fort Collins, Colorado 80523
(Received 14 December 1999)

We investigate rhythmic finger tapping in both the presence and the absence of a metronome. We examine both the time intervals between taps and the time lags between the stimulus tones from the metronome and the response taps by the subject. We analyze the correlations in these data sets, and we search for evidence of deterministic chaos, as opposed to randomness, in the fluctuations.

PACS number(s): 87.19.St, 87.19.Bb, 05.45.Tp, 05.45.Ac

I. INTRODUCTION

Studies of patterns in rhythmic movement have held a special interest in neuroscience and the behavioral sciences because they allow insight into the mechanisms responsible for the emergence of temporal order in the central nervous system and the ability to regulate complex movement and sensorimotor coordination. Although the brain is remarkably adept at producing stable rhythmicity in movement patterns over long periods of time, careful analysis of such time series reveals the ubiquitous and puzzling presence of temporal fluctuations in the control of rhythmic movement [1]. For example, complex temporal fluctuations can be observed in sequential stride-interval patterns [2], finger-tapping periods [3], etc. In rhythmic synchronization tasks, the temporal fluctuations in motor timing create ''noisy'' period and phase relationships between the rhythmic stimulus and the motor response [4,5]. These appearances of randomness or noise in the temporal domain are not limited to the motor system, but, rather, they appear to be a typical and intrinsic manifestation of complex physical and biological systems [6], and the study of the nature of these fluctuations has been the focus of many research efforts [1,7–9].

If we consider a model of the brain as a chaotic dynamical system with nonlinear dissipation [10], we would expect such a system to exhibit a certain amount of erratic fluctuation. An understanding of the inherent properties of these noise patterns would yield considerable insight into the underlying control structure for the timing of rhythmic movement. A remarkable observation, which has not been accounted for sufficiently in purely statistical approaches [11], is how long-range periodic movement patterns are maintained and minuscule or even subliminal perceptual timing adjustments are made with great speed and accuracy within a system exhibiting strong stochastic properties [5,12]. Stochasticity can impose limitations on modeling and prediction, and on understanding the operational measures of a system's behavior. However, much theoretical and empirical research has pointed out potential benefits of the presence of randomness as a critical prerequisite for the dynamical attributes of brain and behavior function. For example, stochasticity may sharpen signal detection (stochastic resonance), prevent entrapment in spurious states, and induce phase trasitions which switch from one state to another [8,13,14]. Thus, the observed temporal fluctuations in time series of rhythmic movement may serve a control function in generating and maintaining rhythmicity, rather than simply corrupting time stability. Another crucial question is whether the fluctuations are truly random or just the result of a deterministic chaotic process.

Recent studies [2,7,15] have shown that stride-cycle fluctuations in gait show long-range power-law correlations. However, these correlations disappeared when stride patterns were cued by a metronome as an external time keeper. The presence of long-range correlations would suggest the presence of some deterministic process in tracking fluctuating time patterns, but follow-up studies regarding the presence and type of deterministic chaos have not been done for these data. Furthermore, gait rhythmicity is believed to be driven physiologically by central pattern generators, reticulospinal neural ensembles with oscillatory output, implying biologically hard-wired rhythm control. In contrast, rhythmic pattern organization can also be achieved in a wide range of movements which are not linked to physiologically rhythmic neural control structures. As an example, for finger tapping in the presence of a metronome, there is rapid adaptation to changes in the metronome pattern, even when these changes are below perception thresholds and well within the range of the variability of the tapping [5,12].

The present study extends the analysis of gait rhythmicity to finger tapping, which involves arm movement and is representative of a different neural control system for motor rhythm. The basic experiment is described in Sec. II, and we analyze the presence of correlations in Sec. III. In Sec. IV, we then search for evidence of deterministic chaos as the source of the randomness in the temporal fluctuations. Finally, we summarize our results in Sec. V.

II. EXPERIMENT

The experiment examines the ability of the human brain to produce periodic arm movement. A periodic series of tones is generated in a set of headphones, and each subject attempts to tap her finger at the same instant as these tones.

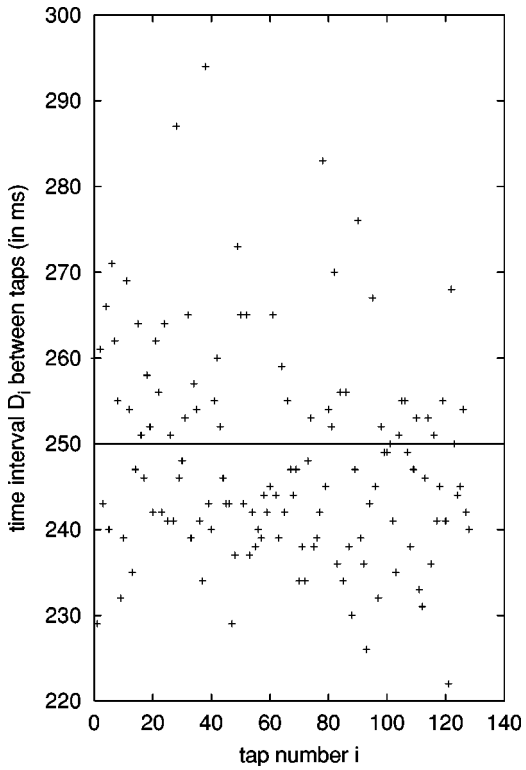

FIG. 1. Differenced time series for a periodic-stimulus experiment. The solid horizontal line at 250 ms indicates the tone period.

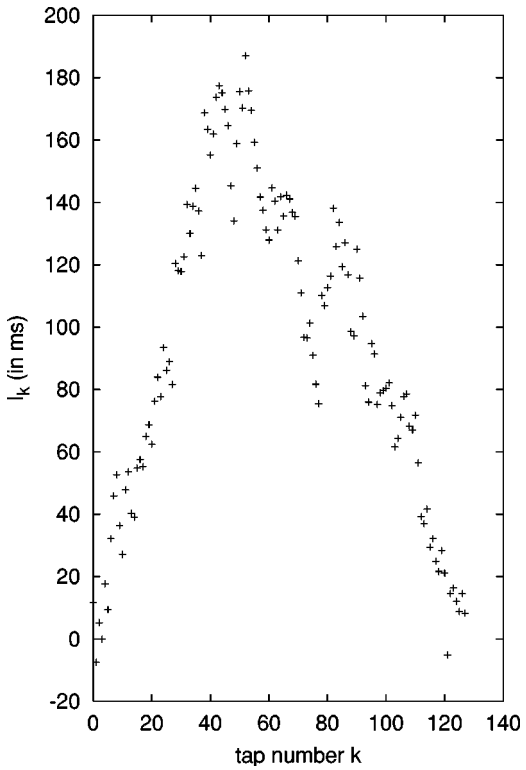

FIG. 2. Integrated time series formed from the differenced data set of Fig. 1.

Each finger tap touches a hand-held electrode to a metal plate, and this allows the time of the tap to be recorded. To collect a set of data, we generate a series of tones, and the subject begins tapping the electrode against the metal plate. The times, in milliseconds, of the tones and the taps are recorded, with the first tone occurring at time $t=0$. The raw data then consist of two columns of numbers, the times of the stimulus tones and times of the response taps.

Two versions of the experiment were performed. In the first version, the periodic series of tones is present for the entire duration of the experiment. This version will be referred to as the periodic-stimulus experiment. In the second version, only ten tones are generated, and the subject then attempts to continue tapping at this periodic rate without having additional tones as a guide. This version will be referred to as the nonstimulus experiment. Each of these two experiments was performed for three different tone periods: 250 ms, 500 ms, and 750 ms. Note that 250 ms is near the natural period for finger tapping in the absence of any external stimulus. While this natural period does vary a bit from person to person, it is generally about four taps per second.

The five subjects were female volunteers whose ages were 28.2 ± 6.9 years. The subjects were healthy and had no known cognitive, perceptual, or neuromuscular disorder. Each subject performed all six of the experiments in two one-hour sessions. Each session was limited to one hour so as to reduce physical fatigue in the forearm and hands, and to reduce mental fatigue from listening to tones in headphones.

III. ANALYSIS OF CORRELATIONS

When a subject first begins tapping her finger, it takes several taps to establish a rhythm. Since we are not concerned with this transient behavior, we discard the first ten data points from each data set. As the subject continues to tap, the time interval between taps tends to vary, and it is these variations that we wish to analyze. In particular, we are interested in the correlations between the variations for successive time intervals.

From the raw data set $\{R_i;i=1,\ldots,N\}$ consisting of the times of the individual taps, we form the differenced data set $\{D_i;i=1,\ldots,N-1\}$, where

$$D_i=R_{i+1}-R_i \tag{1}$$

is the time interval between two successive taps. Figure 1 shows a typical differenced data set for a periodic-stimulus experiment with a tone period of 250 ms.

A. Method for analyzing variations in tapping interval

To analyze the correlations between successive time intervals, we use detrending fluctuation analysis (DFA), which was developed by Hausdorf *et al.* [2] to analyze variations in human gait. We begin by calculating the average tap interval D_{avg} and the deviation of each interval from this average:

$$D_{\text{avg}}=\frac{1}{N-1}\sum_{i=1}^{N-1} D_i, \tag{2}$$

$$\Delta D_i=D_i-D_{\text{avg}}. \tag{3}$$

We then form the integrated time series $\{I_k;k=1,\ldots,N-2\}$ by adding up the first k deviations ΔD_i:

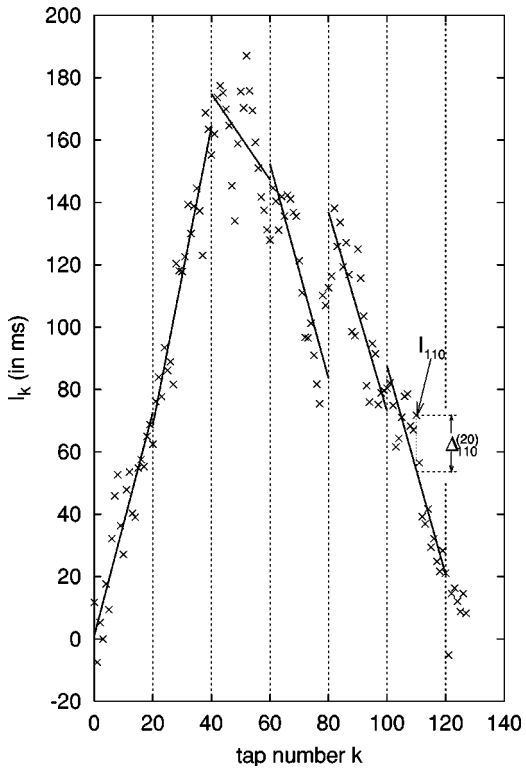

FIG. 3. Least-square local linear fits to the integrated time series of Fig. 2. The interval size of $n=20$ is indicated by the vertical lines, and the lines through the data are the linear fits.

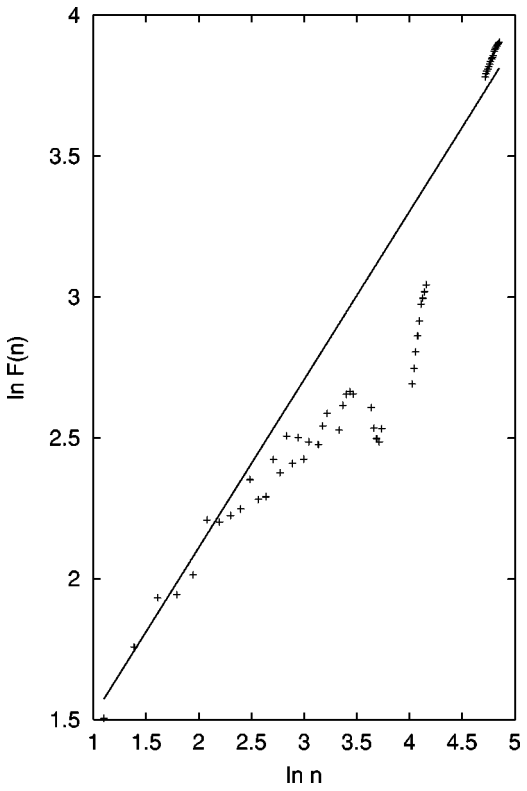

FIG. 4. $\ln F(n)$ versus $\ln n$ for the integrated time series shown in Fig. 2. The slope of the solid line is the scaling exponent γ.

$$I_k=\sum_{i=1}^{k}\Delta D_i \tag{4}$$

(note that $I_{N-1}=0$). Figure 2 shows the integrated time series formed from the differenced data set of Fig. 1.

Next, we examine how well the integrated time series may be fit locally by linear functions. To do this, we divide the horizontal axis into intervals of equal length n, and, for each interval, we find the line which is the best fit to the data (see Fig. 3). We repeat this process for all interval sizes $n=3,4,5,\ldots$. However, not all interval sizes n will divide evenly into the number $N-2$ of data points. Therefore, when we divide the integrated time series into intervals, we attempt to use only the first 120 of the $N-2=128$ data points. For those values of n that do not divide evenly into 120, we then add back the first few data points that were removed from the end of the data set, or we remove a few additional data points, so that the interval size n will divide evenly into the number of data points used. However, if this procedure requires the number of data points used to differ from 120 by more than 8, then that interval size n is not used.

To measure the deviation of the integrated time series from local linearity, we compute the vertical separation $\Delta_k^{(n)}$ between the data point I_k and the local best-fit line (as illustrated in Fig. 3), and then we compute the rms average of these separations:

$$F(n)=\sqrt{\frac{1}{N-2}\sum_{k=1}^{N-2}|\Delta_k^{(n)}|^2}. \tag{5}$$

Repeating this procedure for all interval sizes $n=3,4,5,\ldots$ yields a function $F(n)$ which measures the degree of local linearity over a time interval of n taps [note that $F(n)=0$ unless $n\geqslant 3$, since a linear fit to fewer than three points must be perfect]. As the interval size n increases, the linear fits should become worse, so $F(n)$ should increase. Assuming a power-law behavior $F(n)\sim n^{\gamma}$, the scaling exponent γ may be used to characterize the correlations in the data. According to Hausdorf *et al.* [2], a value of γ between 0.5 and 1.0 indicates persistent long-range correlations.

The exponent γ is the slope of a plot of $\ln F(n)$ versus $\ln n$. Such a plot is shown in Fig. 4 for the integrated time series of Fig. 2. Note that this plot deviates from linearity as n becomes large. This is because of the presence of short-range correlations, and we will discuss this point in more detail in Sec. III D. The procedure for determining the extent of the linear region is also described there.

B. Results of the analysis

We begin by analyzing the periodic-stimulus experiments, where the periodic series of tones is present for the entire duration of each experiment. Each of the five subjects performed this experiment five times at each of three tone periods, 250 ms, 500 ms, and 750 ms. For each of these data sets we calculated a scaling exponent $\gamma_{sj}^{(p)}$, where $s=1,\ldots,5$ indicates the particular subject, p indicates the particular tone period, and $j=1,\ldots,5$ indicates one of the five experiments for that particular subject and that particular period. We then average $\gamma_{sj}^{(p)}$ over the five experiments to obtain

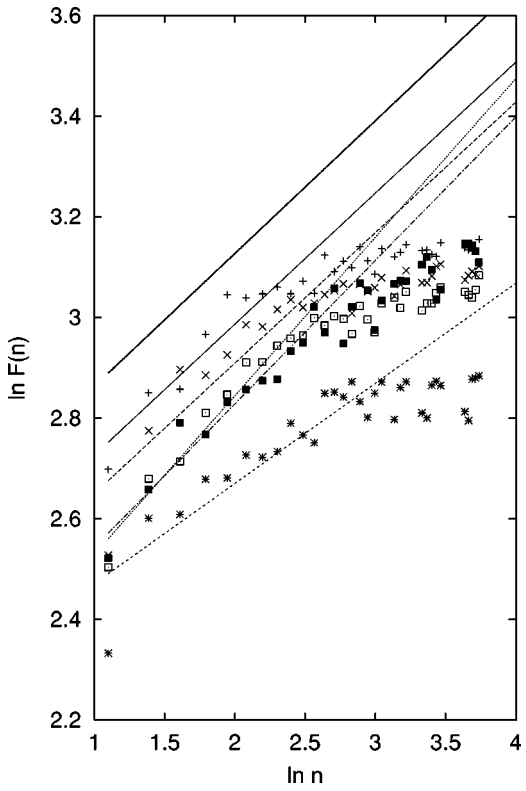

FIG. 5. Plots of $\ln F(n)$ versus $\ln n$ for the five separate periodic-stimulus experiments for one particular subject and a period of $p=750$ ms. The slopes of the five best-fit lines are the five scaling exponents $\gamma_{sj}^{(p)}$, and the average of these five slopes $\gamma_s^{(p)}$ is indicated by the dark line above the five plots.

$$\gamma_s^{(p)}=\frac{1}{5}\sum_{j=1}^{5}\gamma_{sj}^{(p)}, \tag{6}$$

and we average this over all five subjects to determine an average scaling exponent for each period p:

$$\gamma^{(p)}=\frac{1}{5}\sum_{s=1}^{5}\gamma_s^{(p)}. \tag{7}$$

Figure 5 shows the five values of $\gamma_{sj}^{(p)}$ for one particular subject s and a period of $p=750$ ms, as well as the average $\gamma_s^{(p)}$ of these five values. Figure 6(a) shows the five values of $\gamma_s^{(p)}$ and their average $\gamma^{(p)}$ for each of the three periods p. Figure 6(b) shows the corresponding results for the nonstimulus experiments, where the periodic series of tones is stopped after only ten tones, and the subject attempts to continue tapping at this periodic rate without having additional tones as a guide (remember that the first ten taps were considered transient and discarded). In the latter case, the subject does tend to drift from the initial period p, and Fig. 7 shows a typical differenced data set for a nonstimulus experiment. In this particular example, the drift is to shorter periods, but, overall, there did not appear to be any preference between drifting to longer or shorter periods.

Table I lists the six scaling exponents $\gamma^{(p)}$ for the two types of experiment at each of the three periods. Each reported uncertainty is the standard deviation of the five values $\gamma_s^{(p)}$ that were averaged to obtain that particular scaling exponent $\gamma^{(p)}$.

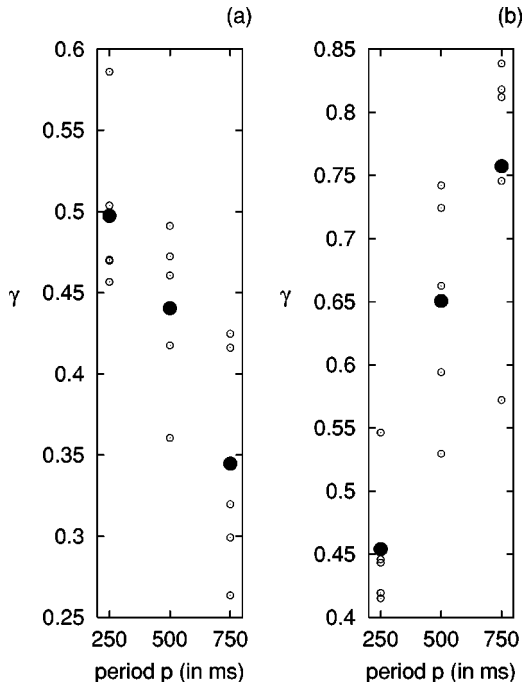

FIG. 6. Scaling exponents γ for the three periods p for the (a) periodic-stimulus and (b) nonstimulus experiments. For each period, the open circles are the values of $\gamma_s^{(p)}$ for the five subjects, and the filled circle is the average $\gamma^{(p)}$ of the five values $\gamma_s^{(p)}$.

We first note that, for a period of 250 ms, the value of γ

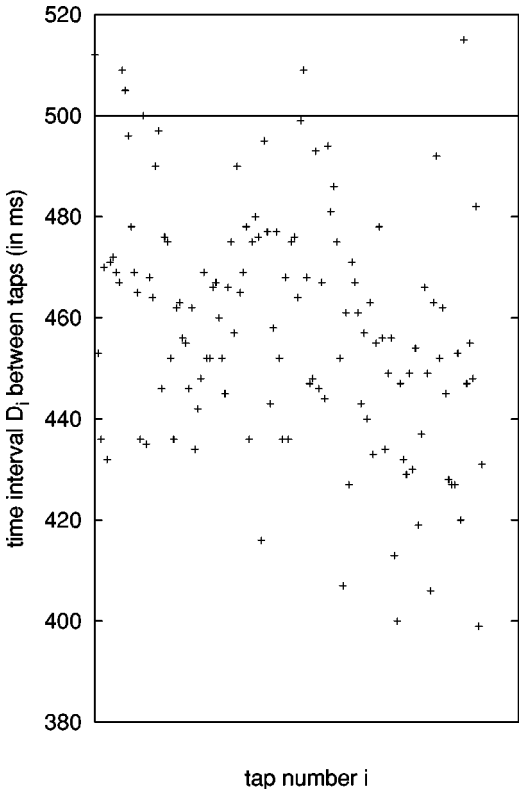

FIG. 7. Differenced time series for a nonstimulus experiment. The solid horizontal line at 500 ms indicates the initial tone period.

TABLE I. Scaling exponents γ.

Type of experient	Period p		
	250 ms	500 ms	750 ms
periodic-stimulus	0.497 ± 0.053	0.440 ± 0.052	0.345 ± 0.072
nonstimulus	0.454 ± 0.053	0.651 ± 0.089	0.757 ± 0.109

TABLE II. Scaling exponents $\tilde{\gamma}$.

Type of experiment	Period p		
	250 ms	500 ms	750 ms
periodic-stimulus	0.324 ± 0.058	0.272 ± 0.086	0.182 ± 0.057
nonstimulus	0.298 ± 0.051	0.514 ± 0.086	0.607 ± 0.098

is the same (within error bars) for the two types of experiments. This is to be expected, since 250 ms is near the natural period for finger tapping, so the presence or absence of the metronome makes little difference. However, as the period increases, we see that γ is between 0.5 and 1.0 for the nonstimulus experiments, indicating the presence of long-range correlations, but it is less than 0.5 for the periodic-stimulus experiments, indicating the absence of long-range correlations. This shows that, in the absence of the metronome, the tapping becomes steady with long-range correlations, but, when the metronome is present, these long-range correlations are broken as the subject attempts to readjust to the most recent tones. When the metronome becomes irrelevant near the natural tapping period, γ must approach the borderline value of 0.5.

For the periodic-stimulus experiments, as the period of the metronome decreases and approaches the natural tapping period of 250 ms, it becomes easier to ignore the metronome and to establish longer-range correlations, so γ increases toward 0.5. For the nonstimulus experiments, as the period increases beyond the natural period, the subject finds it harder to maintain this period. As a result, there is more drift, and the linear fits become worse, causing γ to increase.

C. Modification of the DFA method

In using the DFA method, we divided the horizontal axis of Fig. 3 into intervals of size n and found the best-fit line in each interval. The function $F(n)$ was then the rms average of the vertical separations between the data points and these best-fit lines. However, if short-range correlations exist, then data points near the edge of an interval are less strongly correlated with points near the opposite edge of that same interval than they are with the nearby points in the neighboring interval. Thus, it makes more sense to let $\Delta_k^{(n)}$ be the vertical separation between the data point I_k and the best-fit line for an interval of size n centered about this data point (i.e., there is a different best-fit line for each data point I_k). Note that only odd values of n may be used in this case. However, it is no longer necessary for n to divide evenly into 120 (or a value close to 120).

If short-range correlations exist, then, on average, this modification should reduce the separations $|\Delta_k^{(n)}|$ and their rms average $F(n)$, and this may reduce the scaling exponents γ. Thus, a reduction in these scaling exponents would be evidence of short-range correlations. The scaling exponents $\tilde{\gamma}^{(p)}$ obtained using the modified DFA method are listed in Table II. Note that they are indeed smaller than the previous scaling exponents $\gamma^{(p)}$, which shows that short-range correlations do exist.

D. Correlation length

In Sec. III A, we pointed out that, because of the presence of short-range correlations, the plot of $\ln F(n)$ versus $\ln n$ in Fig. 4 deviates from linearity when n becomes large. This is due to the fact that, when the interval size n exceeds the correlation length, the data near the two ends of the interval become uncorrelated, and the relation $F(n) \sim n^{\gamma}$ ceases to be valid. Thus, the value of n where the plot in Fig. 4 ceases to be linear is an estimate of the correlation length L of the data set.

To find the correlation length L, we begin by selecting a cutoff value $N_c \geqslant 5$ and plotting $\ln F(n)$ versus $\ln n$ only for $n \leqslant N_c$. We then find the best-fit line for this plot, and we let $\chi(N_c)$ denote the rms deviation of the plot from this best-fit line. The average of $\chi(N_c)$ for $N_c = 5$, 6, and 7 is denoted by χ_0, and this is taken as an estimate of the deviation from perfect linearity in the initial linear region. As N_c increases further, so does the ratio $R(N_c) = \chi(N_c)/\chi_0$, and the value of N_c where this ratio exceeds a critical value R_c is taken as the estimate of the correlation length L.

Typical examples of plots of $\chi(N_c)$ versus N_c for the DFA method and the modified DFA method are shown in Figs. 8(a) and 8(b), respectively. For the modified DFA

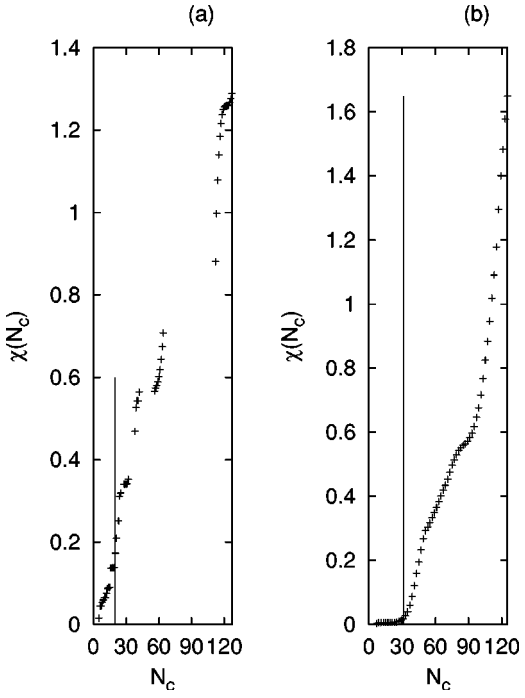

FIG. 8. $\chi(N_c)$ versus N_c for nonstimulus data at 750 ms using (a) the DFA method and (b) the modified DFA method. The solid lines indicate the estimates of the correlation length L using a cutoff of $R_c = 4$.

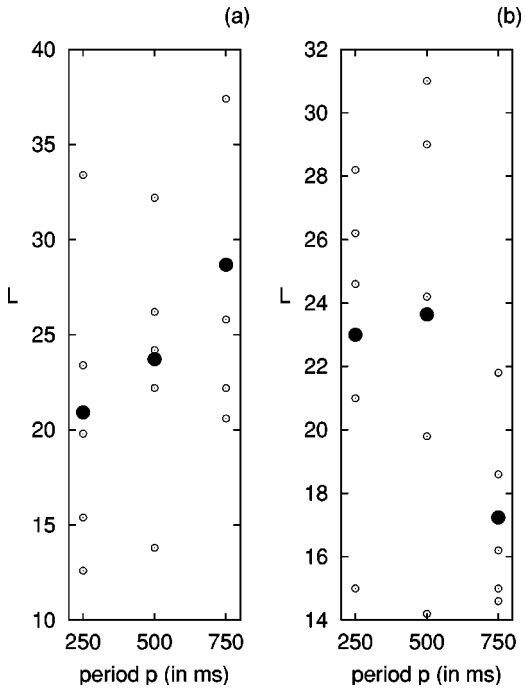

FIG. 9. Correlation lengths L for the three periods p for the (a) periodic-stimulus and (b) nonstimulus experiments. For each period, the open circles are the values of $L_s^{(p)}$ for the five subjects and the filled circle is the average $L^{(p)}$ of the five values $L_s^{(p)}$.

method, the estimate of the correlation length L is quite insensitive to the value of the cutoff R_c, so this is the method that we chose to use. For definiteness, we then chose $R_c=4$.

For each data set, we estimate the correlation length $L_{sj}^{(p)}$, and then we average these values just as we did for the scaling exponents $\gamma_{sj}^{(p)}$:

$$L_s^{(p)}=\frac{1}{5}\sum_{j=1}^{5} L_{sj}^{(p)}, \tag{8}$$

$$L^{(p)}=\frac{1}{5}\sum_{s=1}^{5} L_s^{(p)}. \tag{9}$$

The final results are given in Fig. 9 and Table III. For the periodic-stimulus experiments, the correlation length is independent of the period (within the error bars), which suggests that the subject relies on a fixed number of previous taps, rather than a fixed time interval (note that the three periods vary by considerably more than the error bars for the correlation lengths).

For the nonstimulus experiments, the situation is less clear. The correlation lengths do agree within one standard deviation, but just barely. On the other hand, the corresponding time intervals for the three periods 250 ms, 500 ms, and 750 ms are 5.75 ± 1.30 s, 11.82 ± 3.42 s, and 12.93 ± 2.24 s, respectively, and the latter two values are quite close. This may indicate that there is a transition from reliance on a fixed number of taps to reliance on a fixed time interval if the tapping period becomes large enough. However, investigating this possibility will require collecting data at many more periods, so this is a subject for future study.

TABLE III. Correlation lengths L.

Type of experiment	Period p		
	250 ms	500 ms	750 ms
periodic-stimulus	20.92 ± 8.11	23.72 ± 6.69	28.68 ± 8.18
nonstimulus	23.00 ± 5.19	23.64 ± 6.84	17.24 ± 2.99

TABLE IV. Scaling exponents and correlation lengths for the time lags.

	Period p		
	250 ms	500 ms	750 ms
γ (DFA)	1.04 ± 0.09	0.91 ± 0.11	0.85 ± 0.06
$\tilde{\gamma}$ (modified DFA)	0.93 ± 0.11	0.83 ± 0.13	0.73 ± 0.09
L	16.36 ± 3.23	19.48 ± 5.24	19.08 ± 4.26

E. Analysis of time lags

In the previous sections we analyzed data that were differenced so as to give the time intervals between consecutive taps. However, this is not the only way to difference the data. For the periodic-stimulus experiments, we can also find the time lag between each stimulus tone and the corresponding response tap. The raw data set consists of two columns of data: $\{S_i;i=1,\ldots,N\}$ are the times of the stimulus tones, and $\{R_i;i=1,\ldots,N\}$ are the times of the response taps. We then form the differenced data set $\{\tilde{D}_i;i=1,\ldots,N\}$, where

$$\tilde{D}_i=R_i-S_i \tag{10}$$

is now the time lag between the stimulus tone and the response tap (which may be either positive or negative). Note that we analyze these time lags only for the periodic-stimulus experiments.

Proceeding as before, we obtain the results given in Table IV. Within the error bars, the scaling exponents γ are between 0.5 and 1.0, which indicates the presence of long-range correlations. However, when we analyzed the time intervals between taps for these periodic-stimulus experiments (in Sec. III B), we found that the scaling exponents were less than 0.5, which indicated the absence of long-range correlations. The presence of long-range correlations for the time lags, but not for the time intervals, indicates that the subject adjusts quickly to the correct period, but then eliminates the time lags much more slowly through a gradual drift. This can also be seen from a direct examination of the data.

The additional conclusions are the same as before. The scaling exponent γ again decreases steadily with increasing period. The exponent $\tilde{\gamma}$ is less than the exponent γ, which indicates the existence of short-range correlations. The correlation length L is again independent of the period, indicating a reliance on a fixed number of taps, rather than a fixed time interval.

IV. DETERMINISTIC CHAOS VERSUS RANDOMNESS

The time series in Figs. 1 and 7 appear to fluctuate randomly, but it is possible that these fluctuations are the result of a deterministic process, and that they are chaotic, rather than truly random. This is an important distinction, since a chaotic time series contains a degree of order that is useful for prediction and modeling. In this section, we will use a test developed by Salvino and Cawley [16] to investigate whether the time series are deterministically chaotic or truly random.

A. Time series and embedding

Most systems in nature have a very large number of degrees of freedom, but such systems can often be modeled using only a few relevant variables. For example, a gas consisting of 10^{23} molecules can often be described using only a few variables, such as pressure, volume, and temperature. Once the relevant variables have been determined, the time evolution of the system may be described by a trajectory in a low-dimensional space with these relevant variables as the axes. Although our data sets consist of time series of only a single variable, Takens [17] developed a method for using such data sets to construct a representation of the trajectory in another low-dimensional space which is topologically equivalent to that of the true trajectory. Such a representation is called an embedding of the trajectory, and we now review Takens' method for constructing an embedding from a time series of a single variable.

To construct an m-dimensional embedding from a time series $\{x_i\}$, we select an index lag l, and we form the m-dimensional vectors

$$\vec{v}_i=(x_i,x_{i+l},\ldots,x_{i+(m-1)l}). \tag{11}$$

A plot of the time series $\{\vec{v}_i\}$ in m dimensions will then give the desired embedding of the true trajectory for the system. The quality of this embedding does depend on the chosen values of m and l. For example, if the space for the true trajectory is three-dimensional, but we construct a two-dimensional embedding, then we will obtain a projection of the trajectory onto only two dimensions. Also, the index lag l must not be very short or very long compared to the time scale of the dynamics. In the former case, all of the components of the vector $\vec{v}_i$ will be nearly the same, causing the embedded trajectory to be compressed along a single line. In the latter case, the components of the vectors $\vec{v}_i$ become uncorrelated, and the embedded trajectory does not represent the true underlying dynamics of the system. There is an extensive literature regarding the selection of appropriate values for m and l. However, in using the method of Salvino and Cawley, we need not be concerned with these details.

As an illustration, consider the trajectory in three dimensions generated by the three coupled Lorenz equations [18]:

$$\dot{x}=\sigma(y-x),$$

$$\dot{y}=rx-y-xz, \tag{12}$$

$$\dot{z}=-bz+xy.$$

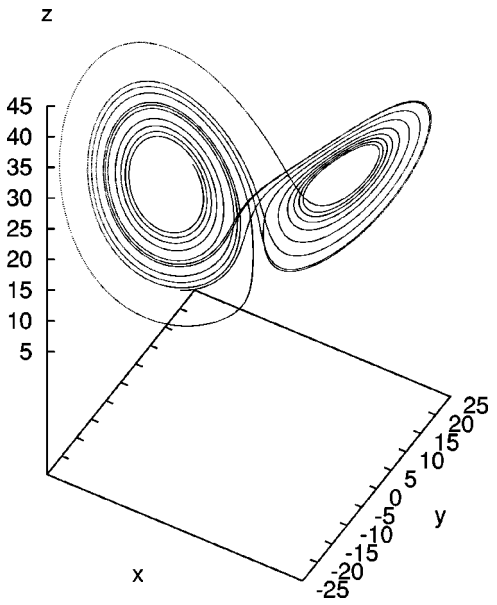

FIG. 10. Trajectory for the Lorenz system [Eqs. (12)] for the parameter values $\sigma=10$, $r=28$, and $b=8/3$.

For the standard parameter values $\sigma=10$, $r=28$, and $b=8/3$, we integrate these equations using a fourth-order Runge-Kutta method with a time step $\delta t=0.001$ to obtain the trajectory shown in Fig. 10. We then construct a time series $\{x_i\}$ by measuring the variable $x(t)$ at the times $0,\tau,2\tau,\ldots$, where $\tau=0.05=50\delta t$. This time series is shown in Fig. 11, and, like the time series in Figs. 1 and 7, it appears to be random. However, we know that it is actually chaotic, since it was generated by the deterministic Lorenz equations. To reconstruct the trajectory from the single time

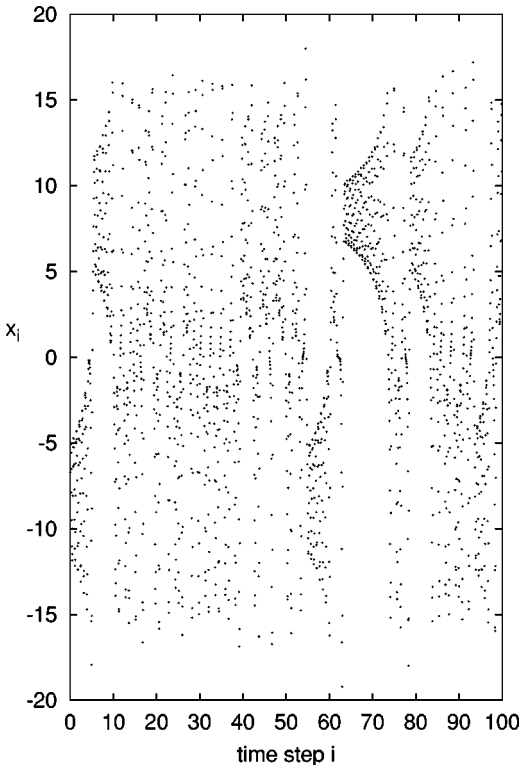

FIG. 11. Time series $\{x_i\}$ for the trajectory in Fig. 10.

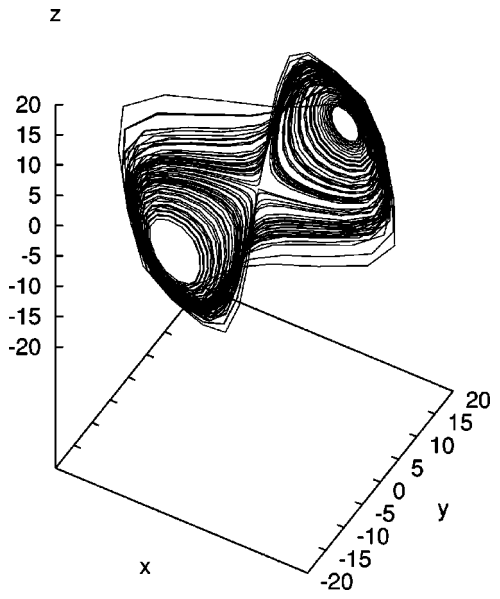

FIG. 12. Reconstruction of the trajectory in Fig. 10 from the single time series $\{x_i\}$ of Fig. 11 using a time lag $l=3$ and an embedding dimension $m=3$. Successive points have been connected by straight lines as a guide to the eye.

series $\{x_i\}$, we form the vectors $\vec{v}_i$ given by Eq. (11), and we plot these vectors as points in m dimensions. Using $l=3$ and $m=3$ yields the embedding shown in Fig. 12, which is topologically equivalent to the true trajectory in Fig. 10.

B. Method for distinguishing between chaos and randomness

The basis for the method of Salvino and Cawley is the fact that a deterministic process generates a smooth trajectory like the one in Fig. 10. As a result, the trajectory reconstructed from the embedding will have a degree of smoothness, rather than hopping around randomly. Thus, we can distinguish deterministic chaos from randomness by measuring the smoothness of the embedding.

In order to illustrate the basic idea, consider the unit tangent vector at each point of the trajectory in Fig. 10. This assignment of a particular unit vector to each trajectory point is a simple example of a vector field, and other assignments of unit vectors to these points produce other vector fields. Since nearby points have nearly the same unit vectors, a local average of these vectors will produce nearly the same vector again, and its length will be nearly 1. However, if the assignment of unit vectors to trajectory points is random, rather than smooth, then, in a local average, these vectors will tend to cancel and yield a net vector whose length is much less than 1. Thus, the length of the local average of the unit vectors in the vector field may be used to distinguish deterministic chaos from randomness.

Salvino and Cawley constructed a vector field by choosing five numbers $c_0, c_1, c_2, c_3,$ and c_4 and then assigning to each embedded trajectory point $\vec{v}_i$ the unit vector

$$\vec{\phi}_i = \sum_{r=0}^{4} c_r \vec{v}_{i+r} \Bigg/ \left| \sum_{r=0}^{4} c_r \vec{v}_{i+r} \right|. \tag{13}$$

In fact, they constructed ten different vector fields using the ten sets of coefficients listed in Table V. Note that the first

TABLE V. Coefficients for the ten different vector fields.

	c_0	c_1	c_2	c_3	c_4
1	−1.0	1.0	0.0	0.0	0.0
2	−3.0	4.0	−1.0	0.0	0.0
3	2.0	−5.0	3.0	0.0	0.0
4	4.7	−3.0	−1.7	0.0	0.0
5	−2.0	3.0	−4.0	3.0	0.0
6	3.5	−2.7	−1.4	0.6	0.0
7	−3.4	−0.5	−0.1	4.0	0.0
8	1.0	2.0	3.0	−4.0	−2.0
9	0.9	0.8	−3.5	4.0	−2.2
10	3.0	−2.0	0.0	2.0	−3.0

vector field produces $\vec{\phi}_i = (\vec{v}_{i+1} - \vec{v}_i)/|\vec{v}_{i+1} - \vec{v}_i|$, which are roughly the same as the unit tangent vectors.

We now partition the m-dimensional embedding space into a uniform grid of small m-dimensional cubes. For each cube, we average the unit vectors $\vec{\phi}_i$ in that cube to obtain the vector

$$\vec{Y}_j = \frac{1}{n_j} \sum_{i=1}^{n_j} \vec{\phi}_i, \tag{14}$$

where j labels the particular cube and n_j denotes the number of trajectory points within that cube. If the embedding is smooth, then the vectors $\vec{\phi}_i$ within a single cube will be nearly the same, so that $|\vec{Y}_j|^2$ will be nearly 1. However, if the embedding is not smooth, then the vectors $\vec{\phi}_i$ within a single cube will point in many different directions, so that they will tend to cancel in the sum, and $|\vec{Y}_j|^2$ will be much smaller than 1. The global average of $|\vec{Y}_j|^2$ is given by

$$W = \sum_j n_j |\vec{Y}_j|^2 \Bigg/ \sum_j n_j . \tag{15}$$

A value of W near 1 indicates deterministic chaos, while a value of W much smaller than 1 indicates randomness.

Since this method relies on having several vectors in each grid cube, then, for a finite number of data points, these cubes cannot be too small. As a result, even for a smooth deterministic trajectory, the vectors $\vec{\phi}_i$ within the same cube will vary somewhat, and W will be less than 1. Also, since the number of vectors in each box will be limited, then, even for a random process, the vectors within each box will not cancel completely, and W will be small, but nonzero. Therefore, we need a concrete criterion for deciding whether W is large enough to indicate determinism or small enough to indicate randomness.

A simple way to test whether a data set is deterministic or random is to see whether or not randomizing it reduces the value of W substantially. However, when we randomize the data set, we do not want to alter its basic distributional properties, such as its power spectrum [i.e., the magnitude of its Fourier transform $F(k)$]. Thus, to randomize a data set, we take the Fourier transform, we then randomize the phases $\theta(k)$, but leave the magnitudes $|F(k)|$ unchanged, and we then take the inverse Fourier transform. The resulting ran-

domized data set is referred to as a surrogate data set. In order for the surrogate data set to remain real, the phase $\theta(k)$ must be odd about $k=0$. Thus, for each $k>0$, we choose $\theta(k)$ to be a random number between $-\pi$ and π, and we then choose the remaining phases by requiring that $\theta(-k) = -\theta(k)$ [and, thus, $\theta(0)=0$]. A fast Fourier transform (FFT) routine was used to calculate the Fourier transforms. As with most FFT routines, it requires the data set to have a size N which is a power of 2.

For the surrogate data set, we again compute the values of W for each of the ten vector fields in Table V. The range of these ten values indicates the range expected for random data sets. We then compute the ten values of W for the original data set. If the original data set is random, then these latter values of W should fall within the same range as the values for the surrogate data set. However, if the original data set is deterministic, then the largest of the ten values of W for the original data set should be significantly above the range of values for the surrogate data set. Since the quality of the embedding depends on the embedding dimension m and the index lag l, we repeat this procedure for a range of values of l, and we check that the results are not dependent on the value chosen for m.

As an example, we analyze a data set consisting of 2048 successive values from the time series $\{x_i\}$ of Fig. 11, which was obtained from the Lorenz system [Eqs. (12)] and used to produce the embedding in Fig. 12. We used an embedding dimension $m=3$ and a grid of $40\times40\times40$ boxes. It should be noted that most of these boxes are empty, and, in computing W, we included only those boxes containing at least three embedded points. The results are shown in Fig. 13, where the two lower curves give the maximum and minimum values of W for the surrogate data set, and the upper curve gives the maximum value of W for the original data set. We see that the maximum value of W for the real data is well above the range of values for the surrogate data set, and this shows that the original data set was generated by a deterministic process.

In general, the separation between the upper curve and the two lower curves is not this dramatic. As another example, we analyze a time series that consists of the particular times at which $x(t)$ for the Lorenz system [Eqs. (12)] reaches a local maximum. Since this samples the trajectory less frequently than does the above example, the evidence of deterministic chaos should not be as strong. This is a more realistic analog to our finger-tapping data, since it consists of the times at which a particular event occurred. The results of this latter analysis are shown in Fig. 14. The number of data points is 2048, the embedding dimension is $m=3$, and the grid consists of $10\times10\times10$ boxes. As in the above example, the lower two curves give the maximum and minimum values of W for the surrogate data set, and the upper curve gives the maximum value of W for the original data set. In this case, the maximum value of W for the original data set is not nearly as close to 1 as in the previous example. In addition, the range of values for the surrogate data set is much larger, and the maximum value of W for the original data set is not as well separated from this range.

C. Results of the analysis

For each subject, period, and experiment type, we initially analyzed each of the five data sets separately. However, those data sets were too small ($N=128$) to satisfy the requirement of having small cubes with several data points in each cube. As a result, we instead concatenated the five data sets to form a single longer data set ($N=640$). We have checked that such concatenation does not alter the results obtained for the Lorenz system [Eqs. (12)]. We have also checked that the method of Salvino and Cawley can detect determinism for such small data sets. For example, the determinism is quite evident for a data set of only $N=512$ points obtained from the Lorenz system with an added noise level of 10%.

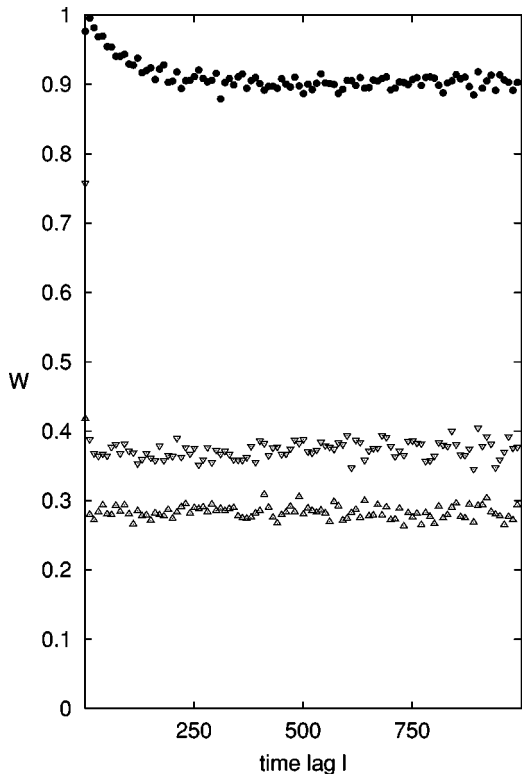

FIG. 13. W versus l for the Lorenz system [Eqs. (12)]. The lower two curves give the maximum and minimum values of W for the surrogate data set, and the upper curve gives the maximum value of W for the original data set.

A typical plot is shown in Fig. 15. Here, we used an embedding dimension $m=2$ and a grid consisting of $27\times27\times27$ boxes, but other choices gave similar results. Also, the plots for other subjects, periods, and experiment types are all similar to this plot, and this is the case for both types of differencing (time intervals and time lags). These plots show no evidence of low-dimensional chaos and instead indicate that the fluctuations are stochastic in nature. This indicates that any model of this system using a small number of relevant variables must include randomness, rather than being purely deterministic.

V. SUMMARY AND DISCUSSION

An analysis of the time intervals between taps shows long-range correlations for the nonstimulus experiments, but not for the periodic-stimulus experiments. This indicates that the presence of the metronome breaks the long-range correlations as the subject attempts to readjust to its most recent tones. On the other hand, an analysis of the time lags be-

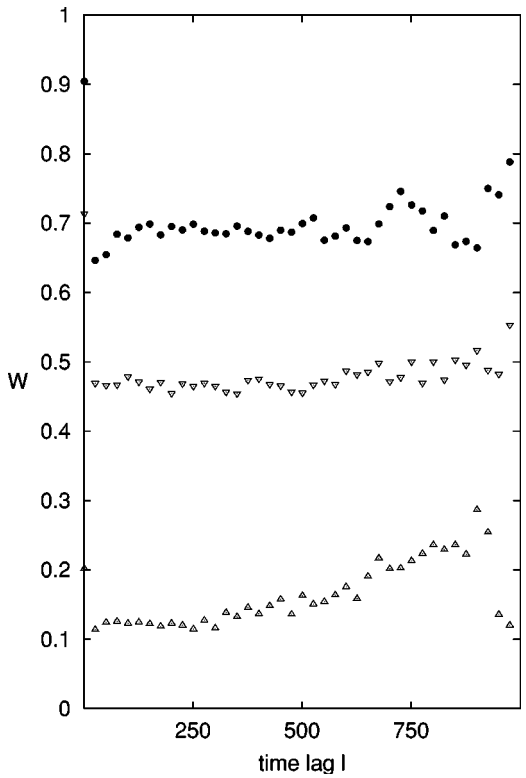

FIG. 14. W versus l for a time series consisting of the times at which $x(t)$ for the Lorenz equations [Eqs. (12)] reaches a local maximum. The lower two curves give the maximum and minimum values of W for the surrogate data set, and the upper curve gives the maximum value of W for the original data set.

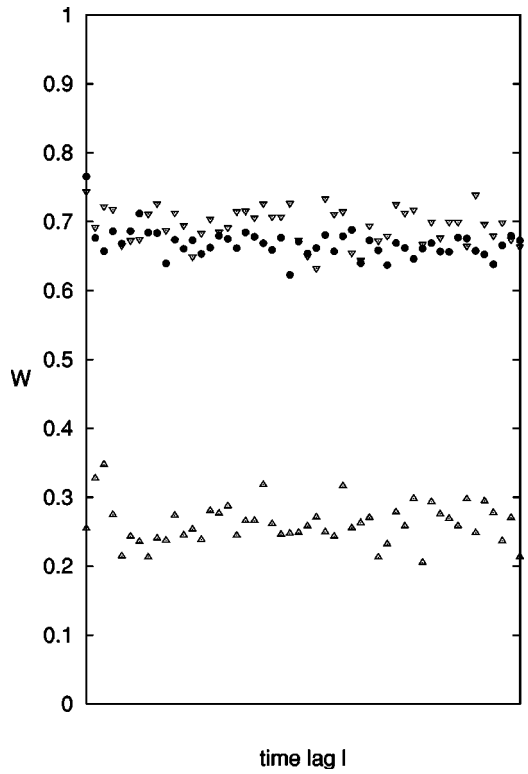

FIG. 15. A typical plot of W versus l for the concatenated data from a single subject for a particular period and experiment type. The lower line is the minimum value of W for the surrogate data set. The maximum values of W for the surrogate data set (inverted triangles) and the original data set (circles) are nearly the same.

tween the stimulus tones and the response taps in periodic-stimulus experiments shows that long-range correlations are present in these data. This indicates that a subject quickly adjusts her tapping period to the metronome period, but then eliminates the time lag (or phase shift) more slowly through a gradual drift.

We also showed that short-term correlations were present in all of these experiments, and we determined these correlation lengths. For the periodic-stimulus experiments, these results indicate that a subject relies on a fixed number of previous taps, rather than a fixed time interval. For the non-stimulus experiments, the results are not as clear, but there is some indication that a subject may rely on a fixed time interval for larger tapping periods.

Although the presence of correlations might suggest that the fluctuations in the data are deterministically chaotic, rather than random, a direct test for determinism failed to demonstrate its presence. One possible explanation for this discrepancy is that the deterministic chaos is not low-dimensional, since our data sets were too small to test for the existence of high-dimensional chaos. However, a more likely explanation is that the fluctuations have the nature of directed Brownian motion, which is random, rather than chaotic, but which also contains correlations. This explanation is also consistent with the conclusion that, in the periodic-stimulus experiments, the time lags between the stimulus tones and the response taps are eliminated by a slow directed drift. Deciding whether or not this is actually the case will require a considerable amount of effort, so this is a subject for future study.

ACKNOWLEDGMENT

This research was supported in part by a Center of Excellence Grant from the Colorado Commission on Higher Education to M. T.

[1] D.L. Gilden, T. Thornton, and M.W. Mallon, Science **267**, 1837 (1995).
[2] J.M. Hausdorf, C.K. Peng, Z. Ladin, J.Y. Wei, and A.L. Goldberger, J. Appl. Physiol. **78**, 349 (1995).
[3] A.M. Wing and A.B. Kristoffersen, Percept. Psychophys. **14**, 5 (1973).
[4] A. Daffertshofer, Phys. Rev. E **58**, 327 (1998).
[5] M.H. Thaut, R.A. Miller, and M.L. Schauer, Biol. Cybern. **79**, 241 (1998).
[6] Y. Chen, M. Ding, and J.A.S. Kelso, Phys. Rev. Lett. **79**, 4501 (1997).
[7] J.M. Hausdorf, P.L. Purdon, C.K. Peng, Z. Ladin, J.Y. Wei, and A.L. Goldberger, J. Appl. Physiol. **80**, 1448 (1996).
[8] J.A.S. Kelso and A. Fuchs, Chaos **5**, 64 (1995).
[9] J.A.S. Kelso, *Dynamic Patterns. The Self-Organization of Brain and Behavior* (MIT Press, Cambridge, 1995).

[10] H. Haken, *Synergetics. An Introduction*, 3rd ed. (Springer, Berlin, 1983).
[11] D. Vorberg and A.M. Wing, in *Handbook of Perception and Action*, edited by H. Heuer and S.W. Keele (Academic Press, London, 1996), Vol. 2, p. 181.
[12] M.H. Thaut, B. Tian, and M.R. Azimi, Human Movement Science **17**, 839 (1998).
[13] A. Fuchs, J.A.S. Kelso, and H. Haken, Int. J. Bifurcation Chaos Appl. Sci. Eng. **2**, 917 (1992).
[14] H. Haken, *Advanced Synergetics*, 3rd ed. (Springer, Berlin, 1987).
[15] J.M. Hausdorf, S.L. Mitchell, R. Firtion, C.K. Peng, M.E. Cudkowicz, J.Y. Wei, and A.L. Goldberger, J. Appl. Physiol. **82**, 262 (1997).
[16] L.W. Salvino and R. Cawley, Phys. Rev. Lett. **73**, 1091 (1994).
[17] F. Takens, in *Dynamical Systems and Turbulence*, edited by D. A. Rand and L.S. Young, Lecture Notes in Mathematics Vol. 898 (Springer, Berlin, 1981), p. 336.
[18] E.N. Lorenz, J. Atmos. Sci. **20**, 130 (1963).